Available online at www.sciencedirect.com
ScienceDirect
Journal of Power Sources 177 (2008) 83–95
JOURNAL OF POWER SOURCES
www.elsevier.com/locate/jpowsour

Diagnosis of PEM fuel cell stack dynamic behaviors

Jixin Chen [1], Biao Zhou *

Department of Mechanical, Automotive and Materials Engineering, University of Windsor, 401 Sunset Avenue, Windsor, Ontario N9B 3P4, Canada

Received 1 October 2007; received in revised form 8 November 2007; accepted 9 November 2007
Available online 21 November 2007

Abstract

In this study, the steady-state performance and dynamic behavior of a commercial 10-cell Proton Exchange Membrane (PEM) fuel cell stack was experimentally investigated using a self-developed PEM fuel cell test stand. The start-up characteristics of the stack to different current loads and dynamic responses after current step-up to an elevated load were investigated. The stack voltage was observed to experience oscillation at air excess coefficient of 2 due to the flooding/recovery cycle of part of the cells. In order to correlate the stack voltage with the pressure drop across the cathode/anode, fast Fourier transform was performed. Dominant frequency of pressure drop signal was obtained to indicate the water behavior in cathode/anode, thereby predicting the stack voltage change. Such relationship between frequency of pressure drop and stack voltage was found and summarized. This provides an innovative approach to utilize frequency of pressure drop signal as a diagnostic tool for PEM fuel cell stack dynamic behaviors.

Keywords: PEM fuel cell; Pressure drop; Frequency; Dynamic behavior; Diagnostic tool

1. Introduction

The PEM fuel cell has been regarded as an ideal power source for a variety of applications due to its significant advantages, *i.e.*, high efficiency, low emission, silence and simplicity [1]. Presently, the PEM fuel cell is the top contender under research and development compared with other mainstream types of fuel cells. This is mainly because the PEM fuel cell has high power density and low operating temperature. Due to the complex physics behind PEM fuel cell electrochemistry, the dynamic behaviors of PEM fuel cell have not been fully studied and understood. Also, the transience of PEM fuel cell after start-up/load-change is more difficult to model than the steady-state performance. It has been gradually realized that studies on the dynamic behaviors is extremely important as the fuel cell stack will always experience transience during start-up, shutdown and switch of power requirement in portable and automotive applications. Identification of the physics behind the dynamic behaviors, the proposal of diagnostic tools and corresponding control method during transience will provide potential solutions for improving stack durability, efficiency and optimizing system development.

Many modeling studies on PEM fuel cells have been performed. In this paper, the authors focus on the dynamic modeling studies. One of the earliest dynamic models was developed by Amphlett et al. [2], which predicted the cell voltage, power and stack temperature as a function of time when the stack experienced perturbations. They considered the stack as a whole (without consideration of temperature gradient and local current variation) to develop the model as it was the earliest attempt in modeling study. Shan and Choe [3] developed an improved dynamic model for PEM fuel cell stack considering temperature effects. They conducted simulations to analyze start-up behaviors and the performance of the stack in conjunction with the cells. Yan et al. [4] extended their previous steady model of reactant transport to an unsteady one, which was employed to examine the transient transport characteristics and the system performance of PEM fuel cells. Their model was based on the assumption of two-dimensional mass transport in the cathode. Recently Shimpalee et al. [5,6] used a commercial computational fluid dynamics (CFD) solver to simulate the transient response of a PEM fuel cell subjected to a variable load and particularly focused on the overshoot/undershoot behavior under different flow stoi-

* Corresponding author. Tel.: +1 519 253 3000x2630; fax: +1 519 973 7007.
E-mail address: bzhou@uwindsor.ca (B. Zhou).
[1] Present address: Department of Mechanical and Aerospace Engineering, University of California, Irvine, CA 92697, USA.

0378-7753/$ – see front matter © 2007 Elsevier B.V. All rights reserved.
doi:10.1016/j.jpowsour.2007.11.038

chiometry conditions. Their modeling study was based on their previous experimental observation of overshoot/undershoot in transience [7,8]. Yu et al. [9] developed a water and thermal management model to study the steady-state and dynamic performance of a Ballard® PEM fuel cell stack, a commercially available product. Their results showed the stack taking about 30–40 min to reach the steady-state conditions, which was further verified by the real operation. Wu et al. [10] considered four main transient processes in a PEM fuel cell including species transport, electric double layer charge/discharge, membrane hydration/dehydration and heat transfer and proposed a rigorous transient model accounting for all four transient mechanisms. Their model, although adopting a two-dimensional modeling domain, is one of the most comprehensive and advanced currently available in the literature. Wang and Wang [11,12] developed a three dimensional dynamic model considering all the important transient processes in PEM fuel cells including gas transport, water accumulation in the membrane and double layer discharge. Their model is also one of the most advanced in open literature, which features the prediction of overshoot/undershoot during step changes under some operating conditions.

Experimental studies on PEM fuel cell dynamic behavior are few in open literature. Hamelin et al. [13] studied the transience of a PEM fuel cell under fast load communications and reported the faster fuel cell system response time than the load communications. Kim et al. [7,8] reported the influences of reservoirs, fuel dilution and gas stoichiometry on the dynamic behaviors during load changes and they observed the overshoot/undershoot of the current density during cell voltage switch. This is an important phenomenon that indicates the physics of the dynamic behaviors of PEM fuel cells, however it is still not well understood and controlled. Recently Yan et al. [14] conducted an investigation on the dynamic behaviors of PEM fuel cells under a series of changing parameters, *i.e.*, the feed gas humidity, temperature, feed gas stoichiometry, air pressure, fuel cell size and flow channel pattern. The authors reported that all of those parameters have significant influence on the transient response. Although they provided an overall experimental data for validation of related fuel cell models, they did not focus on any parameter to further identify the effects on the transience. Philipps et al. [15] explored the behaviors of a dynamically operated large-scale (11.5 kW) fuel cell system. Their research showed that a power-dependent modulation of the feed gas pressure and flow rate was necessary to achieve high energy efficiency.

It should be noted that although a number of experimental studies have been performed on dynamic behavior of PEM fuel cells and found in the literature, the research is still at initial stages. Most publications display the bulk experimental data during the transience under various operating conditions. Nonetheless, the significant physics that produces the unique transient response observed in the experiments, such as water flooding and removal, have not been thoroughly studied and understood. On the other hand, studies on the dynamic behaviors of a PEM fuel cell stack are limited in the literature compared with those involving a single cell. Dynamic behavior of a single cell and a stack is completely different, which can be theoretically explained by the more complicated mass transport, local current distribution and water management. Such difference has also been experimentally observed [14]. For example, it is evident that for dynamic behavior of a fuel cell stack, one or several cells may experience serious output decay while others remain in normal status, which is detrimental to the stack durability. Therefore, it is necessary and worthwhile to investigate the dynamic behaviors of a stack so as to provide experimental data for stack design and system control. Finally, the unstable voltage has been observed as a significant phenomenon in dynamic behavior. However, few studies have focused to correlate such voltage change in transience with pressure drop across cathode/anode, which is potentially a diagnostic tool for controlling stack output. Barbir et al. [16] and He et al. [17] conducted preliminary studies on pressure drop as a diagnostic tool for water flooding in PEM fuel cell. Nevertheless, they investigated steady cases only and did not explore the general relationship between pressure drop and cell voltage. Consequently, their methodology and conclusion may not be applicable to different cases although as a preliminary investigation their findings were of great significance. Numerically, Jiao et al. [18,19] reported the unsteady pressure drop across the stack using FLUENT® aided simulation, which was correlated with the liquid water transport behavior. Their study suggested that the pressure drop oscillation could be utilized as a diagnostic tool for water behavior. There is hardly any other publication in literature that concerns pressure drop as a diagnostic tool in fuel cell operation. A more thorough study on pressure drop as a diagnostic tool in dynamic stack operation is thus very necessary, which not only aids the understanding of physics in stack dynamic behaviors but also extends the previous research with regard to pressure drop.

2. Experimental

In the present study a 10-cell commercial PEM fuel cell stack from Palcan Power Systems Inc., was operated under a variety of conditions using the self-developed PEM fuel cell test stand. The authors would like to note that the overall performance of the commercial stack under test was not satisfactory with respect to the maximum attainable current density. Conversely, the purpose of the study was to explore the physics behind such phenomenon thus is not aimed to show the superiority of the design of this fuel cell stack.

2.1. Experimental setup

A PEM fuel cell test stand was self-developed as part of the project. It can monitor and/or control all operating parameters relating to PEM fuel cell performance including mass flow rate of the reactants, absolute pressure of the reactants, pressure drop across cathode/anode, stack temperature, gas temperature at inlet/outlet, humidity of the reactants before entering the stack, current drawn from stack and stack voltage and power. It features self-developed LabVIEW codes that is friendly interfaced with users, which can implement the instrument control, display and record data in a real-time format, and monitor the necessary parameters to prevent potential danger such as stack overheating. Not only the steady-state performance, but also the dynamic

Table 1
Mass flow rate setting for steady-state cases

	Air flow rate (SLPM)	Hydrogen flow rate (SLPM)
Case 1	1.47, 1.97, 2.48, 2.95	0.603
Case 2	2.48	0.497, 0.623, 0.828

behavior of PEM fuel cell can be investigated with the aid of the test stand due to its programmable instrument control and data logging features.

2.2. Steady-state cases

To investigate the steady-state performance, the electronic load was set to work under constant current mode. The current was increased from 0.5 A to the maximum value the stack could draw, with a step variance of 0.5 A. The voltage was recorded when it stabilized. In case 1 (refer to Table 1), the air flow rate was varied whereas hydrogen flow rate was kept constant; in case 2, the hydrogen flow rate was varied whereas air flow rate was kept constant. The system pressure during operation was 1 local atmosphere (the same for all other cases below) since both anode and cathode were open to the atmosphere. Mass flow rates and current drawn from the stack were controlled, whereas the stack voltage, temperature and humidity were determined by the electrochemistry and system configuration (the same for all other cases below). The current density was calculated at a given effective MEA area of 36 cm^2.

2.3. Start-up cases

To investigate the stack start-up characteristics (refer to Table 2), the stack was started from idle to 1 A, 2 A, 4 A, 6 A current load, respectively, with stack voltage monitored and recorded. Based on the operating experience in the steady-state cases, it was difficult to draw currents higher than 6.5 A from the stack. Therefore those current setpoints represent different load levels. For every case, the mass flow rates of reactants were determined by excess coefficient, 2 for air and 1.2 for hydrogen. The definition of excess coefficient at a given current load is as follows [20]:

$$\lambda = \frac{\text{actually supplied mole number of air (oxygen) or hydrogen}}{\text{theoretically consumed mole number of air (oxygen) or hydrogen}}$$

These excess coefficient values were selected in such a way that the stack voltage oscillations would be induced, which was the focus of the study because the authors wanted to investigate the physics behind such behavior.

Table 2
Mass flow rate setting for start-up cases

	Start-up load level	Excess coefficient for air	Excess coefficient for hydrogen
Case 1	From idle to 1 A load	2	1.2
Case 2	From idle to 2 A load		
Case 3	From idle to 4 A load		
Case 4	From idle to 6 A load		

Table 3
Mass flow rate setting for current step-up cases

	Current step	Excess coefficient for air	Excess coefficient for hydrogen
Case 1	From 1 A to 2 A From 1 A to 3 A From 1 A to 4 A From 1 A to 6 A	1.5	1.2
Case 2	From 1 A to 2 A From 1 A to 3 A From 1 A to 4 A From 1 A to 6 A	2.0	1.2
Case 3	From 1 A to 2 A From 1 A to 3 A From 1 A to 4 A From 1 A to 6 A	3.0	1.2

2.4. Current step-up cases

Current step-up cases were performed in a similar fashion with the start-up cases. Instead of idle, the stack was first stabilized at 1 A current load, followed by increasing the current setpoint to 2 A, 3 A, 4 A, 6 A, respectively. For both air and hydrogen, the excess coefficient remained unchanged before and after current step-up. Thus the mass flow rate setpoints were increased together with the current setpoint at the moment that was referenced as zero. Table 3 summarizes the approach. The air excess coefficient was varied in every sub-case whereas the hydrogen excess coefficient was kept constant. This was because the hydrogen excess coefficient had very limited influence on the stack dynamic behaviors as long as it was higher than 1.1.

3. Results and discussions

3.1. Steady-state cases

As shown in Fig. 1, the overall steady-state performance improved with the increase in the air flow rate. At low current

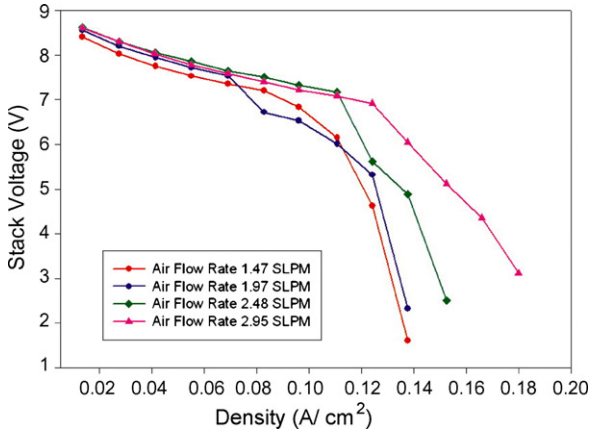

Fig. 1. Stack polarization curve under different air flow rates.

density, the difference was not obvious since even the lowest air flow rate (1.47 SLPM) corresponded to an excess coefficient higher than 4. At elevated current densities, the difference became apparent. Since humidification of incoming gases was performed via the water collected in the humidifier at the downstream of the cathode outlet, incoming gases to the stack were not fully humidified to 100% RH. Usually only 60–80% RH was reached. This contributed to the low current density, however it was not the major contributor.

It should be noted that the final sharp drop of stack voltage at current densities higher than 0.13 A cm^{-2} was not attributed to the mass transport loss or drying out of membrane, which is usually the reason for a single cell operation. Here such sharp drop was an indication that several cells became inactive or "dead" (generating cell voltage lower than 0.1 V) at elevated current density. Actually other cells, which were still working properly, maintained a satisfactory voltage output of 0.6–0.8 V. For example, in the case of 2.95 SLPM for air flow rate, the stack voltage was 3.1 V at current density of 0.18 A cm^{-2}. This did not indicate an average cell voltage of 0.31 V for all 10 cells, and the fact was that only four cells were working at about 0.7 V as an average, others being inactive. Such phenomenon was attributed to the fact that at elevated current those inactive cells suffered from flooding. In other words, very few or no reactants passed through those flooded cells due to their higher flow resistance compared with those under normal operation. This uneven distribution of mass flow rate to different cells was a unique characteristic in stack operation, which will be further discussed in the dynamic behavior section below. A higher air flow rate is therefore preferred in terms of better removal of water and prevention of flooding.

Fig. 2 shows that the hydrogen flow rate had very limited influence on the stack performance. Since the hydrogen supply rate was sufficient to maintain the reaction, the sharp drops in stack voltage observed in all cases were due to the inactive cells at elevated current load. In other words, the stack performance was still determined by air flow rate. The same air flow rates resulted in similar final stack voltage, *i.e.*, three normally working cells.

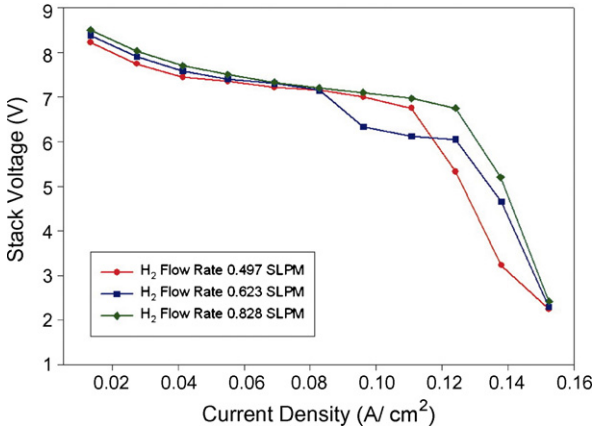

Fig. 2. Stack polarization curve under different hydrogen flow rates.

3.2. Start-up cases

3.2.1. Stack voltage responses

Fig. 3a shows how the stack voltage changed with time when the stack was started from idle to 1 A load. The air flow rate was low due to the low current load given a fix excess coefficient. With the reaction moving forward, additional water was generated but not removed smoothly due to the unknown problems in gas channel design and fabrication, as well as the low air flow rate. In addition to humidifying the membrane, liquid water accumulated and then flooded the electrode. Gradually, additional cells became inactive and stack voltage was observed to experience sudden sharp drop when one more cell malfunctioned. Because of the low air flow rate, or, its low capacity to remove liquid water, inactive cells could not recover. When there were only five cells working, the stack voltage appeared to stop decreasing. This indicated that in addition to the electrodes, cathode gas channels in those non-working cells may have been also blocked by liquid water so that air could hardly pass through those cells. The average air flow rate at the channels of the remaining five cells was therefore increased, which explains why those cells no longer suffered from electrode flooding. Finally, the stack voltage was observed to be stable with five cells working.

Fig. 3b and c (start-up to 2 A and 4 A, respectively) presents obvious voltage oscillation compared with Fig. 3a. At an elevated current load, the air flow rate was higher given the same excess coefficient. The reason for the oscillation is that the air flow rate was not high enough for several (not all) cells to be always maintained without flooding; whereas the air flow rate was high enough so that if too many channels were blocked by water (total gas channel cross-section area reduced and average air flow rate increased), one or two inactive cells could recover when liquid water in the gas diffusion layer/channel being removed by air flow. The non-working cell during the oscillation may be arbitrary based on the observation in experiments, *i.e.*, one newly flooded cell may cause another one that was previously inactive to recover. This can be attributed to the fact that although the average air flow rate was increased, it is arbitrary to determine the cell in which water was first removed. As soon as water in one cell's channel was removed, the average flow rate reduced and probably no additional cell could further recover due to insufficient air flow rate.

As shown in Fig. 3d, the stack voltage response from idle to 6 A load is similar to previous cases except that finally the stack voltage fell down to zero, all cells being flooded resulting in cell inactivity. The final drop began at around 1800 s after start-up. It should be noted that after half an hour operation at high current, there was substantial amount of water accumulated in the GDL and/or gas channel. Consequently, the increase of average air flow rate due to generation of inactive cells (as explained above) was no longer sufficient to remove flooding water in other cells as in low current level cases. Furthermore, as the air flow could only pass through the remaining working cells, the average flow rates at such cells were greatly increased. The authors would like to point out that during voltage oscillation, such average flow rate increase also existed, as analyzed

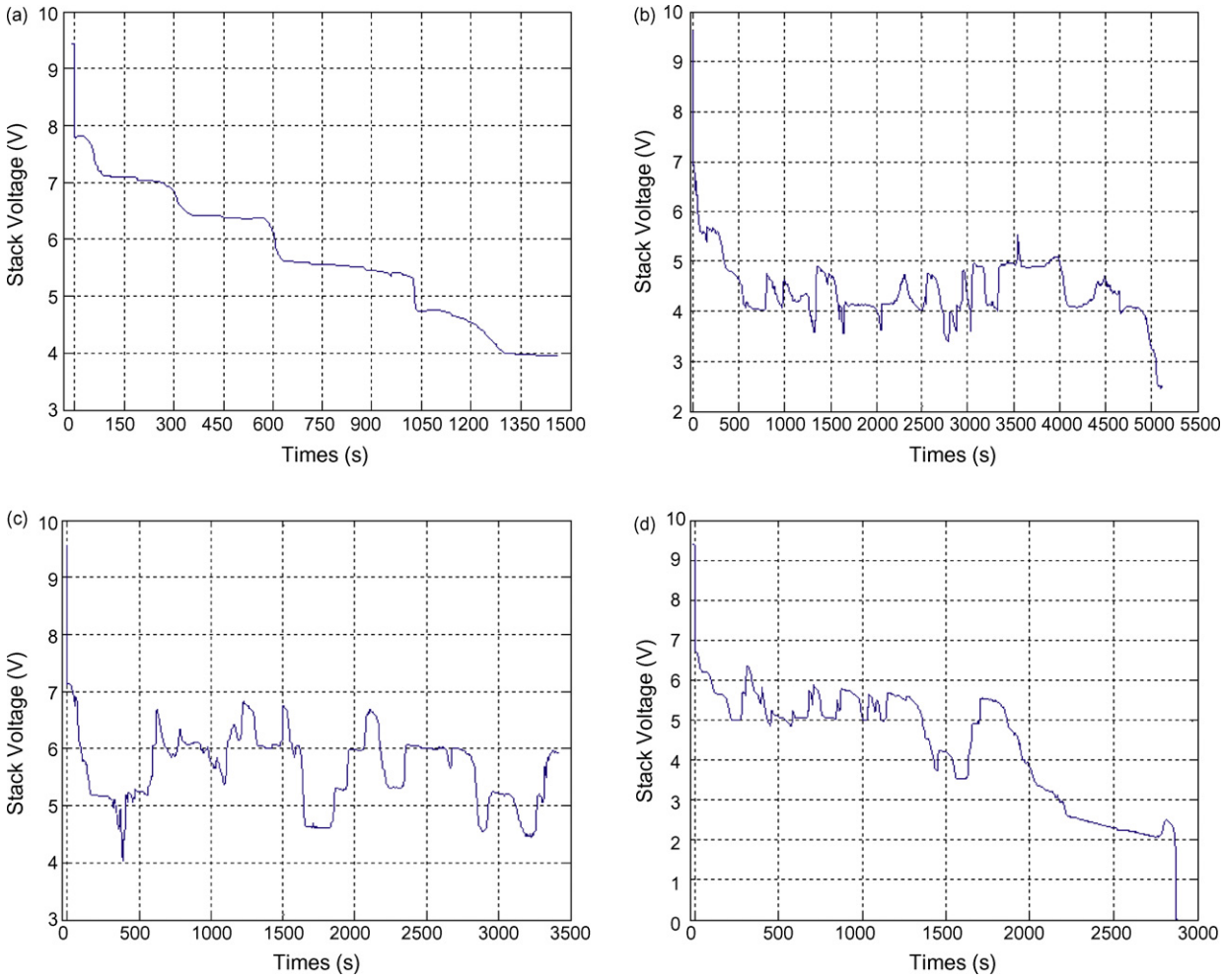

Fig. 3. (a) Stack voltage response when stack started from idle to 1 A load; (b) stack voltage response when stack started from idle to 2 A load; (c) stack voltage response when stack started from idle to 4 A load; (d) stack voltage response when stack started from idle to 6 A load.

in previous paragraphs. However, the recovery of flooded cells immediately offset such increase. As mentioned, such recovery did not occur during the voltage drop after 1800 s. The effect of average flow rate increase, therefore, only imposed on those remaining working cells, resulting in increased flow rate in those cells. The unsteady flow-induced non-uniform local current may generate a great amount of water locally in a short time, which could flood the cell locally. Although the average current was fixed, the local current may vary due to the extremely high flow rate resulted from uneven flow rate passing through the channel. The non-uniform distribution in local current could accelerate when local flooding occurred; finally the whole cell was flooded. This may explains the quick voltage decay to zero after 1800 s.

3.2.2. *Pressure drop responses in time domain*

Fig. 4a shows the cathode (air)/anode (hydrogen) pressure drop changes when the stack was started to 1 A load. The cathode pressure drop kept increasing since the average air flow rate at the opening channels was increasing when additional channels became blocked and the cells inactive. It is supported by the fact that the relatively abrupt increase of cathode pressure drop at around 600 s and 1050 s corresponds to the stack voltage drop at the same time in Fig. 3a. For the anode pressure drop, in addition to those numerous small oscillations, which will be explained later, there were several large and apparent oscillations, as one can see before 600 s and 1050 s. Again, such undershoots relate to the stack voltage drop at that time. Because new inactive cells appeared at those moments due to cathode electrode flooding, the hydrogen consuming rate, or, the rate of hydrogen ion generation at the catalyst sites was reduced before those moments. The time delay between tack voltage drop and decrease of anode pressure drop could be explained as follows: when the cathode gas diffusion layer was blocked by water, there was a certain amount of air left at the catalyst layer, which could still sustain the reaction for a while. Hence the stack voltage would not immediately drop. However, as soon as the gas diffusion layer was blocked, the reaction rate at the cathode catalyst layer was reduced since oxygen was not replenished any longer; thereby reducing the hydrogen ion concentration gradient in the membrane (unconsumed hydrogen ion accumulated). As a result, the reactions that hydrogen was oxidized to hydrogen ions at anode catalyst layer would become much slower. As the hydrogen flowed through the electrode without (or with minimal) consumption, the anode pressure drop reduced abruptly. Further-

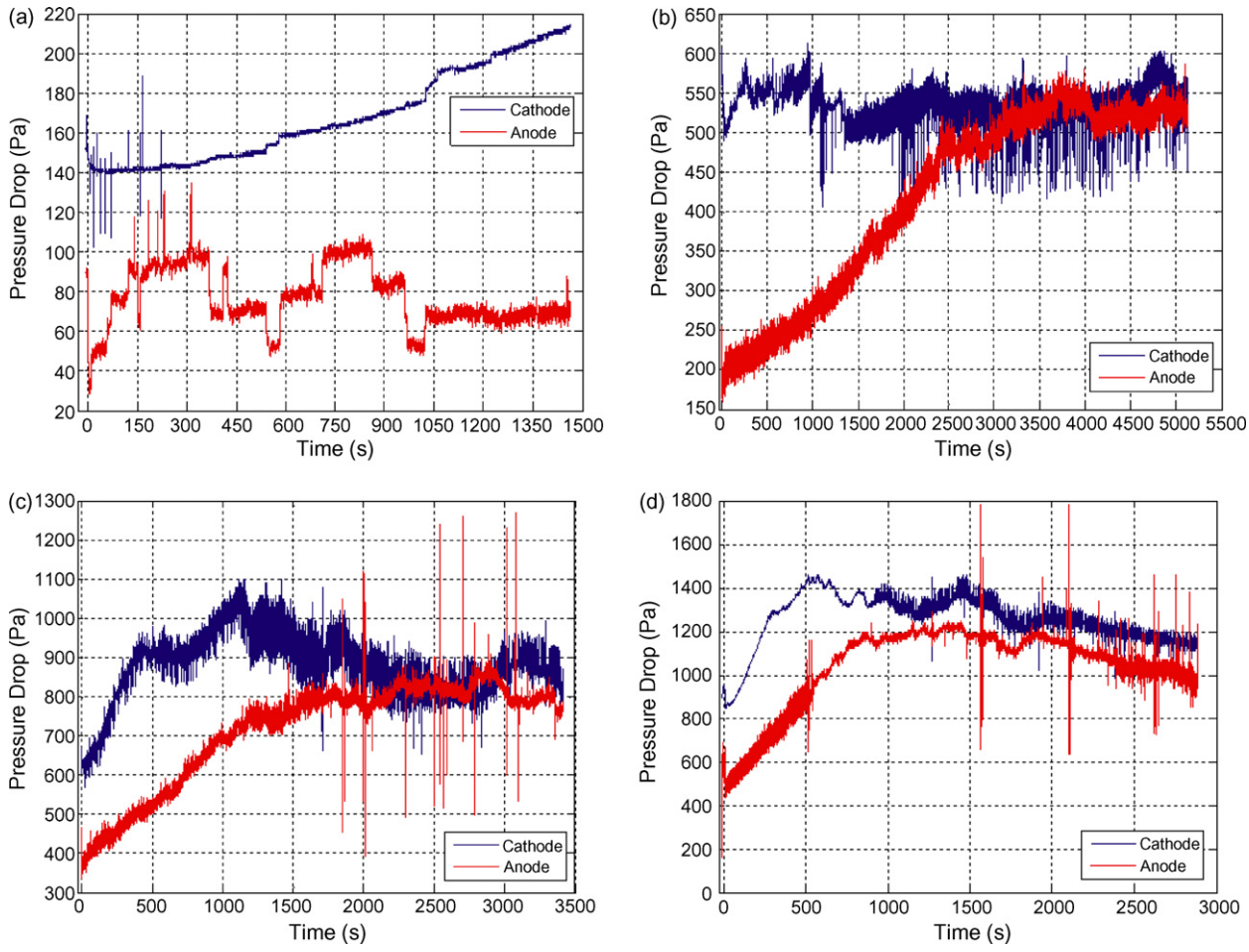

Fig. 4. (a) Change of pressure drop with time when stack started from idle to 1 A load; (b) change of pressure drop with time when stack started from idle to 2 A load; (c) change of pressure drop with time when stack started from idle to 4 A load; (d) change of pressure drop with time when stack started from idle to 6 A load.

more, the immediate increase of anode pressure drop after the undershoot was attributed to the back diffusion of liquid water to the anode, which concurrently flooded the anode. The liquid water in the anode gas diffusion layer and/or channel would hinder the hydrogen flow, thereby increasing the pressure drop. Finally, the authors would like to address the abrupt increase of the anode pressure drop right after 300 s, which corresponds to the stack voltage drop at that time. Note that the cathode pressure drop did not experience abrupt increase at around 300 s, which suggests this stack voltage drop started from the anode flooding instead of cathode. It seems to be unusual; however considering that the stack had just started for 5 min, the liquid water resulting anode flooding may be the remaining water in the system after previous operation.

Fig. 4b–d show the pressure drop changes when the stack was started to higher current loads. The pressure drop signals in these cases contained increased frequency and high-peak oscillations compared with Fig. 4a (notice the pressure drop axis scale). Unfortunately, such signals could hardly be analyzed in the time domain, much information being masked by oscillation. Essentially, the high-frequency oscillation was due to the liquid water in the system. At elevated current, increased amounts of water could be present and the reactant flow disturbed more arbitrarily and frequently. Overall, such signals could still be analyzed without too many details. For example, in Fig. 4b the anode pressure drop increased with time before 4000 s due to the increase of water amount at anode, experienced an undershoot at around 4000 s due to the inactive cell generated at that time, similar to the case of start-up to 1 A load. However, such overall analysis is insufficient.

3.2.3. *Dominant frequency of the pressure drop signals*

To combat this problem, the authors turned to the frequency domain, aiming to find the relationship between pressure drop and stack voltage. Signals are converted from time domain to frequency domain through the Fourier transform. It converts the signal information to a magnitude and phase component of each frequency. Customarily the Fourier transform is converted to the power spectrum, which is the magnitude of each frequency component squared. The spectrum can be investigated to obtain information of which frequencies are present in the input signal and/or which are significant components.

A fast Fourier transform (FFT) is an efficient algorithm to compute the discrete Fourier transform (DFT). For the pressure drop signal, it was sampled every 0.16 s and recorded in the data file. Therefore it could be considered a discrete data

sequence and FFT can be performed, although the pressure drop itself was an analog signal. The details of FFT algorithm is not presented here as in the study it was performed simply by related Matlab commands without knowing the internal workings.

To process the pressure drop data through FFT technique, the authors would like to first introduce two self-defined parameters. "Window" is the data to be processed together by FFT. For every start-up case, the duration was at least 1500 s; every 0.16 s there was a pressure drop data, totally amount of data was therefore tremendous. One needs to determine how many data to be processed at once so that the optimum power spectrum that facilitates analysis could be generated. The amount of data is termed "window size". In Matlab codes developed for processing pressure drop data using FFT, the authors applied the algorithm that in every consecutive seven data, take the first one as the "window center", that is, half of the window size applied to the data right before the center and half to after the center. In this way that point of data became the center of the window. Taking first data out of every consecutive seven as the window center was to separate window centers by 0.96 s, roughly 1 s (time between two consecutive data is 0.16 s). At each window center, identical data was captured (half window size) before and after to form one FFT processing object.

Note that the power spectrum obtained after performing FFT on the window would have numerous frequency components that show different power. The frequency having maximum power obviously is the major component. However considering only the frequency at maximum power may not be reasonable especially when the second maximum power is very close to the maximum. Here the authors defined a parameter to describe the major frequency component, which is termed "dominant frequency" of the pressure drop signal:normalized dominant frequency $= f_1 \times \frac{P_1}{P_1+P_2+P_3} + f_2 \times \frac{P_2}{P_1+P_2+P_3} + f_3 \times \frac{P_3}{P_1+P_2+P_3}$ where P_1 is the maximum power and f_1 the corresponding frequency, P_2, P_3 the second and third maximum power and f_2, f_3 is the corresponding frequencies.

The normalized dominant frequency indicated the major frequency component by taking the frequencies with the largest three powers into account.

Starting from zero, window centers were located at the start of every 0.96 s, where FFT were performed given a specific window size. However, the window size could not be applied to all window centers from zero to the end. If the half of the window size was larger than the amount of all available data between the zero and window center, for example, the window center was located at 0.96 s after start-up whereas the half window size was 20 data, which corresponds to $20 \times 0.16 = 3.2$ s, then the half window size changed to the amount of all data between zero and window center (0.96 s), with window size doubled. This algorithm also applies if the window center is approaching the end of time period for data recording, *i.e.*, if the half window size is larger than the distance between end of time period and window center in terms of amount of data/time, the distance between automatically becomes the half window size.

Ultimately, the plot of time versus normalized dominant frequency could be obtained at a time step of 0.96 s. Algorithms mentioned above and the plotting was performed by Matlab codes. It should be noted that such plot was not unique since the window size had not been specified. Different window sizes may generate different plots. Take an example of start-up to 1 A case (revisit Fig. 3a). As illustrated in Fig. 5 , the dominant frequency of cathode pressure drop versus time plots are presented in terms of different window sizes.

First, it should be noted that the maximum frequency did not exceed 3.125 Hz, which is half of the sampling frequency of the pressure drop data ($1/0.16 = 6.25$ Hz). Such maximum frequency is also called Nyquist frequency in FFT algorithm. This relationship has to be followed for performing FFT. The normalized dominant frequency calculated by the largest three frequency components is obviously within the same range.

As shown in Fig. 5, a very small window size would produce unwanted noise or oscillations so that useful information was still masked, whereas too large window size would reduce frequency peaks and remove some relatively low peaks, which may be a loss of important information. A medium window size, which is 504 data in this case, was the optimum, all major peaks being shown but hardly noise. The criteria for window size selection can be summarized as:

(1) show less noise (unless the oscillation cannot be removed even with a large window size, which means dominant frequency does oscillate with time);
(2) retain significant peaks, especially those that are potentially correlated with stack voltage increase/decrease;
(3) small window size is preferred if above two being satisfied simultaneously, because small window size means less delay if feedback control is performed to stabilize the stack voltage. Also, small window size results larger frequency peaks that are retained, which is preferred by testing instrument.

The above criteria apply to dominant frequency plots in all start-up and current step-up cases. For other cases, only the plot generated under the optimum window size was presented, *i.e.*, the comparison and selection process would no longer show due to the limited space. The following figures put together the dominant frequency and stack voltage plots with time. As mentioned, the purpose was to establish the relationship between pressure drop frequency and stack voltage, which is not so clear if pressure drop signal analyzed only in the time domain. Instead, the pressure drop signal was first processed in frequency domain to obtain the dominant frequency. Such frequency is expected to correlate with stack voltage response during start-up. The authors would like to also emphasize that the dominant frequency does not mean the physical changing frequency of the pressure drop signal; it only indicates the major frequency component of a series of samples. The focus of this study was the relative trend of frequency change and not individual frequency values, which is variable over different window sizes and sampling rates.

3.2.4. Dominant frequency of cathode pressure drop versus stack voltage

As shown in Fig. 6a, when the stack was started from idle to 1 A load, the stack voltage drop, or, generation of the inactive cell was predicted by one or several frequency peaks before. Frequency peaks indicated that the water began to flood the gas diffusion layer and gas channel. Air flow was disturbed and pressure drop became unstable, as can be found around 450 s. Then the frequency became almost zero, which means air no longer passed through this flooded cell. However, the stack voltage was maintained for a while, because (1) the air left in electrode sustained the reaction for a while at low current; (2) small volt-

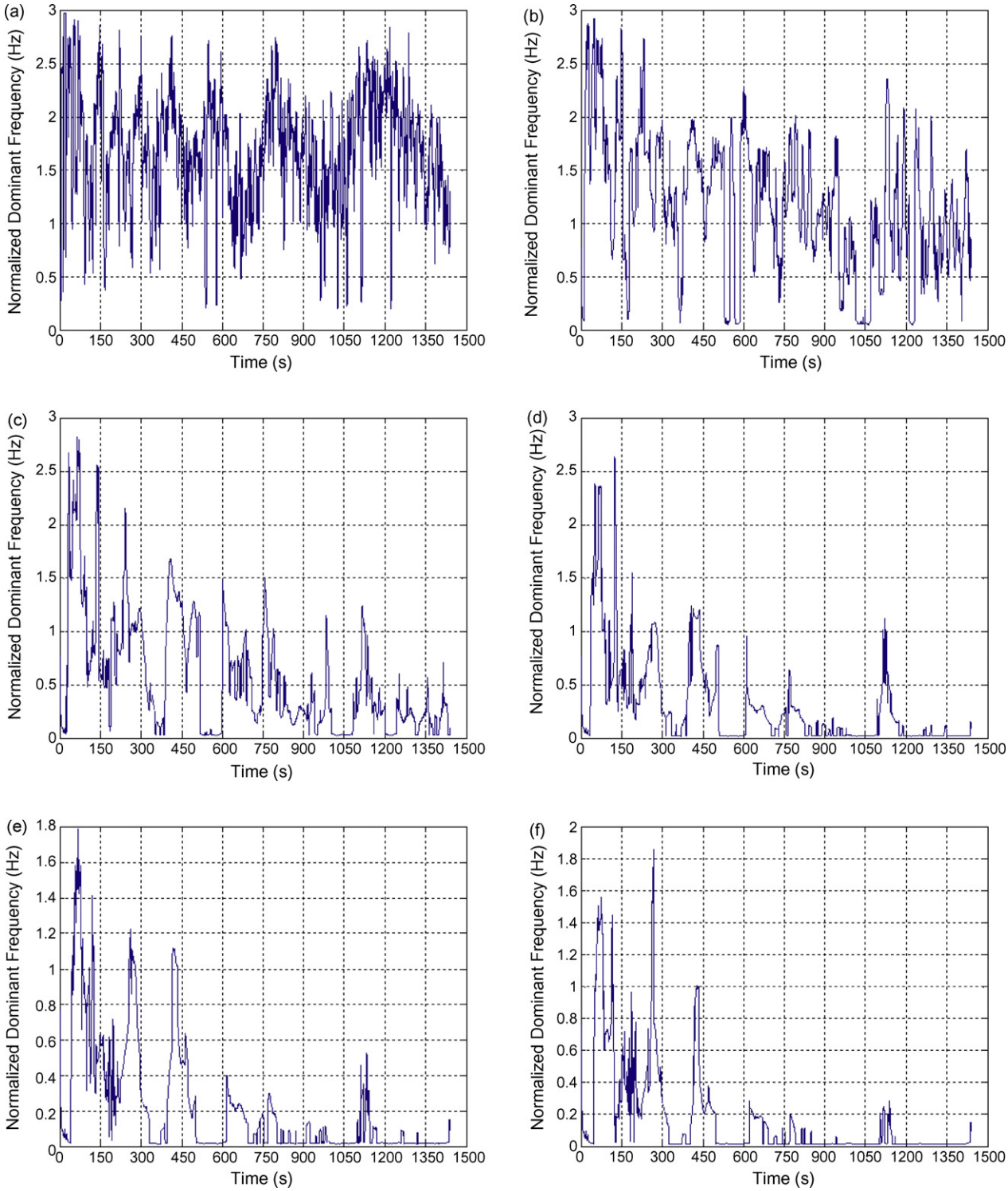

Fig. 5. Dominant frequency vs. time plots under different window sizes ((a) window size 36 data, or 5.76 s; (b) window size 144 data, or 23.04 s; (c) window size 288 data, or 46.08 s; (d) window size 432 data, or 69.12 s; (e) window size 504 data, or 80.64 s; (f) window size 576 data, or 92.16 s; (g) window size 720 data, or 115.20 s).

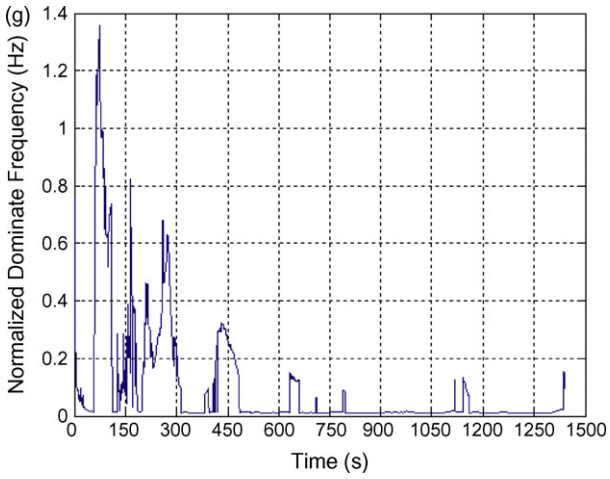

Fig. 5. (*Continued*).

age reduction in this flooded cell was compensated by voltage increase of other cells under a higher average air flow rate. After 600 s another cell began to suffer flooding, which caused the unstable pressure drop again. For this cell, it took a longer time to be fully flooded, a series of frequency peaks being the evidence. The abrupt stack voltage drop also appeared later than frequency becoming almost zero. Again, although the air did not pass the flooded cell, its cell voltage saw a gradual decrease at first and then the abrupt drop after a while. Both the frequency peak and flat bottom can be used as the diagnostic tool

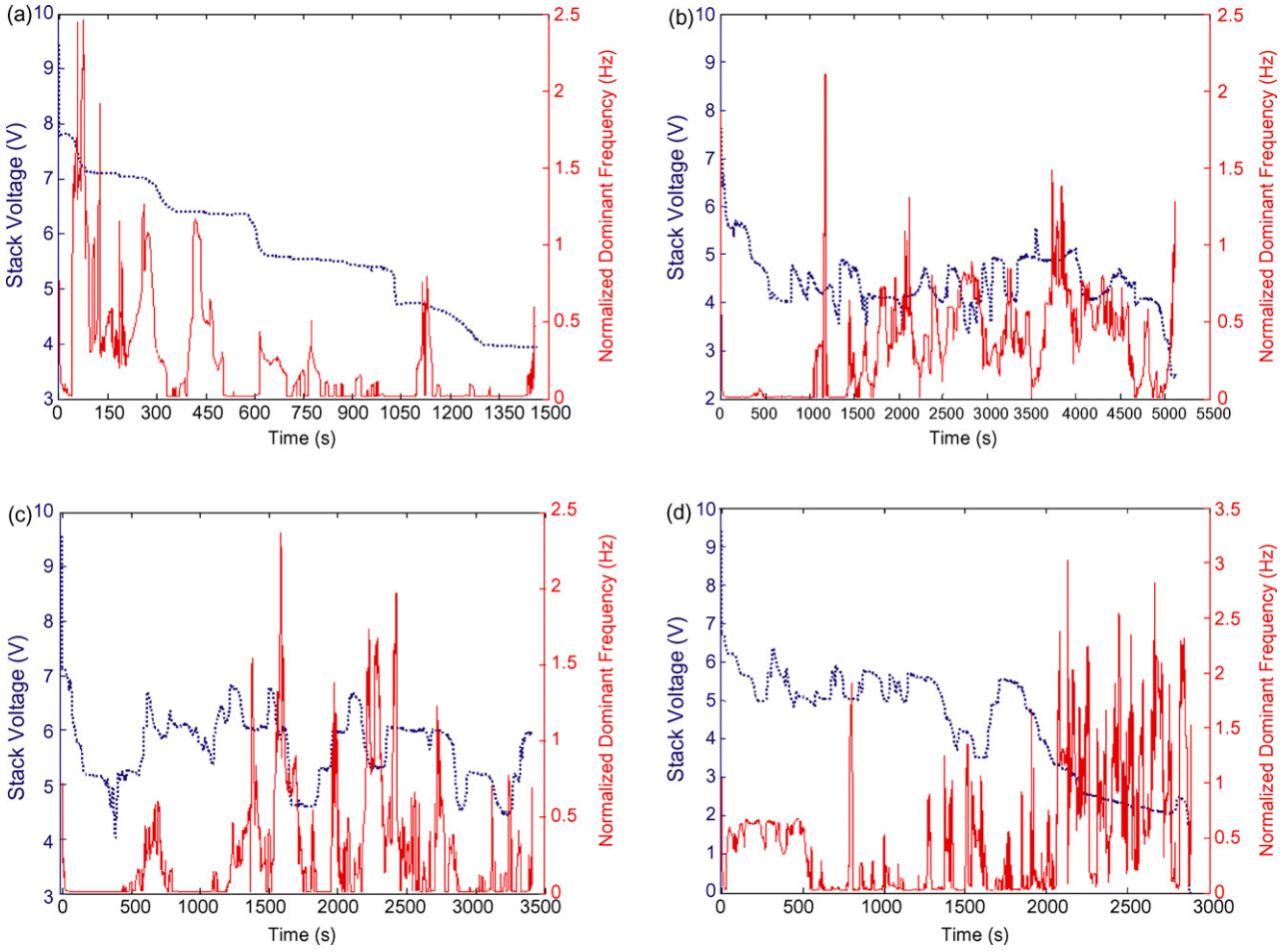

Fig. 6. (a) Changes of dominant frequency of air/cathode pressure drop and stack voltage with time when stack started from idle to 1 A load; (b) changes of dominant frequency of air/cathode pressure drop and stack voltage with time when stack started from idle to 2 A load; (c) changes of dominant frequency of air/cathode pressure drop and stack voltage with time when stack started from idle to 4 A load; (d) changes of dominant frequency of air/cathode pressure drop and stack voltage with time when stack started from idle to 6 A load.

for in-process flooding and cease of air flow to the flooded cell, respectively. It should be addressed that the initial and final frequency peaks are due to the algorithm regarding the window size. Also, there may be some liquid water left in the stack that caused the frequency peaks before 150 s. The system was always unstable at initial start-up due to the low stack temperature and liquid water left inside from previous operation. As a result, the frequency plot at the beginning and end may be ignored in the analysis as a diagnostic tool.

As shown in Fig. 6b, frequency change with time in 2 A load start-up case was much more complicated. The initial flat bottom of low frequency was attributed to the increased air flow rate in this case, which may be capable of removing the remaining water in the channels rapidly. On the other hand, fresh water generated via the reaction was too less to influence the air flow at initial start-up. Consequently, the pressure drop was relatively stable for approximately 1000 s. The initial stack voltage drop was due to the unstable electrochemistry and warming up status right after start-up.

After 1000 s, the frequency began to oscillate. Every peak corresponds to the in-process flooding in the gas diffusion layer and channel. As mentioned before, the stack voltage oscillation was because the air flow was capable of removing the water in one or two flooded cells if too many cell channels were blocked. Therefore, the bottoms of frequency oscillation were the indication that one or two cells that were flooded previously had recovered after the water was removed. Notice the stack voltage and dominant frequency signals from 2000 s to 3500 s approximately, these two signals present a roughly 180° phase delay relationship if modeled by a sine function, *i.e.*, the peak of stack voltage corresponds to the bottom of frequency and vise versa. The water flooding-removal cycle essentially determined the phase reverse of these two signals. Similarly in this case, a stable stack voltage with one or several simultaneous frequency peaks predicted an abrupt voltage drop after a period of time.

Fig. 6c shows that in 4 A start-up case, the frequency oscillation also occurred with even more higher peaks. This can be explained by the fact that at 4 A load, more water was generating, imposing more disturbance on the air flow. Again, the reverse phase of stack voltage signal and frequency signal was observed.

As shown in Fig. 6d, initially it took almost 1000 s for the frequency to start the oscillations. This is because, at 6 A load the air flow rate was high (2 SLPM), small amount of water was readily removed and could not disturb the air flow until the reaction rate increased with stack temperature, sufficient water being capable to flood the cell. The stack voltage oscillation before 1000 s may be related to the unstable and uneven mass transport, since there was still certain amount of water, either freshly generated or previously left, in the gas diffusion layer. Here it is shown again that initially after start-up, the frequency information may not be well utilized as a diagnostic tool for stack voltage. In this case, finally the stack voltage fell to zero and the load was shutdown owing to the flooding in all cells. During the final voltage drop to zero, frequency saw a series of intense oscillations obviously due to the great amount of water in the channel. The air flow still passed the stack, probably through several cells whose channels were not fully blocked, but being highly disturbed by water and unable to reach the catalyst layer.

3.2.5. Dominant frequency of anode pressure drop versus stack voltage

Fig. 7a–d present the anode pressure drop frequency changes with time for different start-up cases. Increased amount of oscillations were observed compared with the cathode pressure drop. The frequency peaks, again, were due to the water disturbance in the channels or even gas diffusion layer. For hydrogen, such disturbance was more obvious since its momentum was much lower than air. As a result, even though there was only small amount of water at the anode, the frequency saw the oscillation. When more water was present at the anode (see the areas of final voltage drop in Fig. 7a, b, and d), such oscillation became increasingly apparent. However, due to the sensitivity of hydrogen pressure drop to water and the fact that water at anode was usually from cathode back diffusion, it may not be good practice to use frequency of anode pressure drop as a diagnostic tool for the stack voltage. It is preferred to focus on cathode pressure drop as the diagnostic tool.

3.3. Current step-up cases

3.3.1. Stack voltage responses

3.3.1.1. Non-oscillation cases. In cases 1 and 3 in Table 3, stack voltage oscillation was not observed during current step-up. Stack voltage reached the new steady-state after a period of time.

Figs. 8 and 9 show the stack voltage responses in non-oscillating cases. As shown in Fig. 8, when excess coefficient for air was 1.5, before the current step the stack voltage stabilized at about 2.4 V, indicating that only three cells were not flooded. It appears that air flow at excess coefficient of 1.5 was unable to remove the flooding water at any current load thereby maintaining the steady-state of the stack. After the current step-up, it took several minutes to stabilize, still only three cells being active. When excess coefficient for air was 3, which means the air flow was strong enough to remove flooding water, the steady-state was also achievable. As shown in Fig. 9, before the current step at least nine cells were active with a total voltage of 7–7.6 V. However, after step-up the stack voltage either increased (1–2 A and 1–3 A cases) due to recovery of one cell, or decreased due to inactivity of one flooded cell (1–4 A case) or the elevated current (1–6 A case). The flooding was still observed at one cell, and it could not recover later. That is why the oscillation was not observed when the air excess coefficient was high. It could be attributed to the fact that the air flow removed water in other nine active cells and maintained the reaction. The air flow could not pass through the flooded cell due to its increased flow resistance.

3.3.1.2. Oscillation cases. As shown in Fig. 10a–d, when the air excess coefficient was fixed at 2, oscillations occurred similar to the observations in the start-up cases, which could be as well considered as responses under current step-up starting from zero. The authors concluded that the air excess coefficient or flow rate determined the stack voltage oscillations. The air excess coeffi-

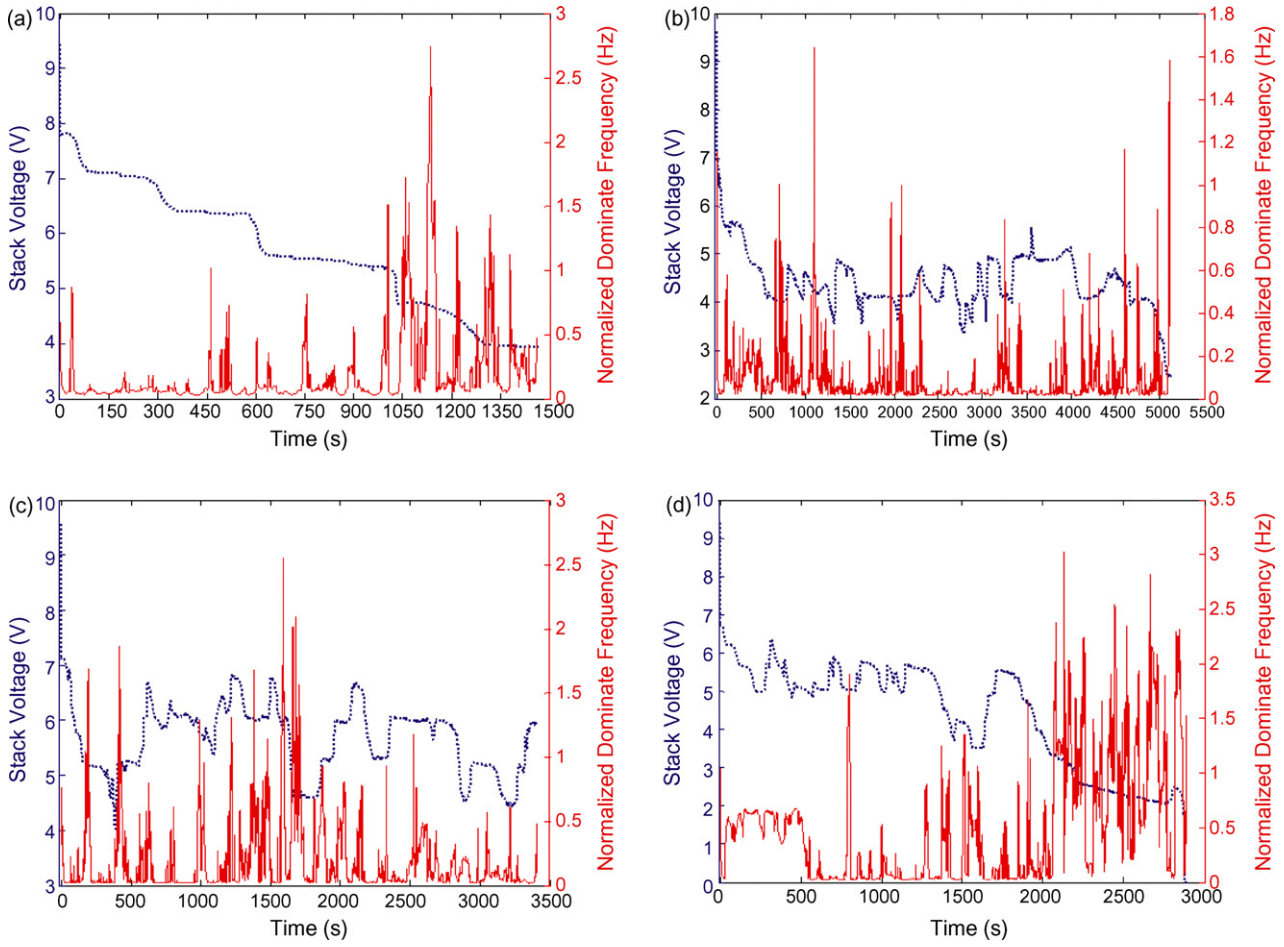

Fig. 7. (a) Changes of dominant frequency of hydrogen/anode pressure drop and stack voltage with time when stack started from idle to 1 A load; (b) changes of dominant frequency of hydrogen/anode pressure drop and stack voltage with time when stack started from idle to 2 A load; (c) changes of dominant frequency of hydrogen/anode pressure drop and stack voltage with time when stack started from idle to 4 A load; (d) changes of dominant frequency of hydrogen/anode pressure drop and stack voltage with time when stack started from idle to 6 A load.

cient must be at a medium level to oscillate the stack voltage. For instance, an excess coefficient of 2 is standard value for air in fuel cell industry; however, from the observations it is suggested a higher value may be preferred for stack operation, although the oscillations may also be attributed to the design and manufacturing problems specifically for this stack. In addition, operation experience gained in the current step-up cases in turn provided the authors some hint that the start-up cases should be run at

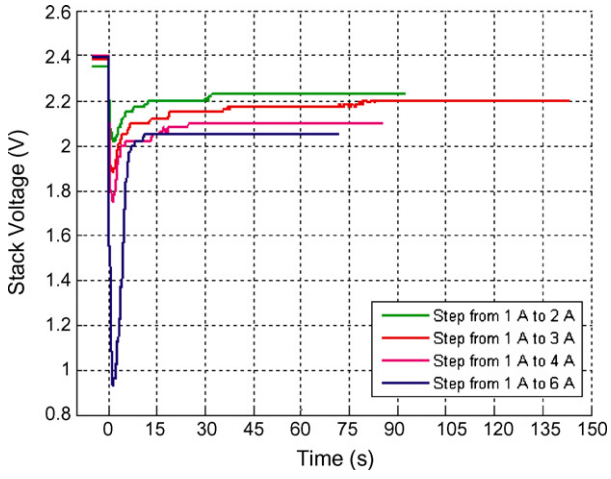

Fig. 8. Stack voltage responses after current step-up with excess coefficient fixed at 1.5 for air and 1.2 for hydrogen.

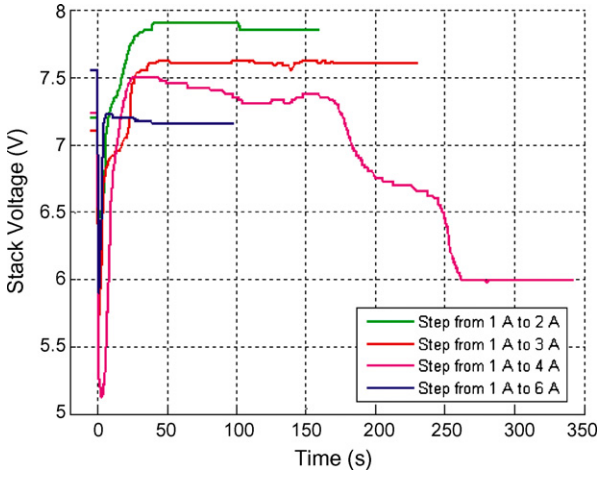

Fig. 9. Stack voltage responses after current step-up with excess coefficient fixed at 3 for air and 1.2 for hydrogen.

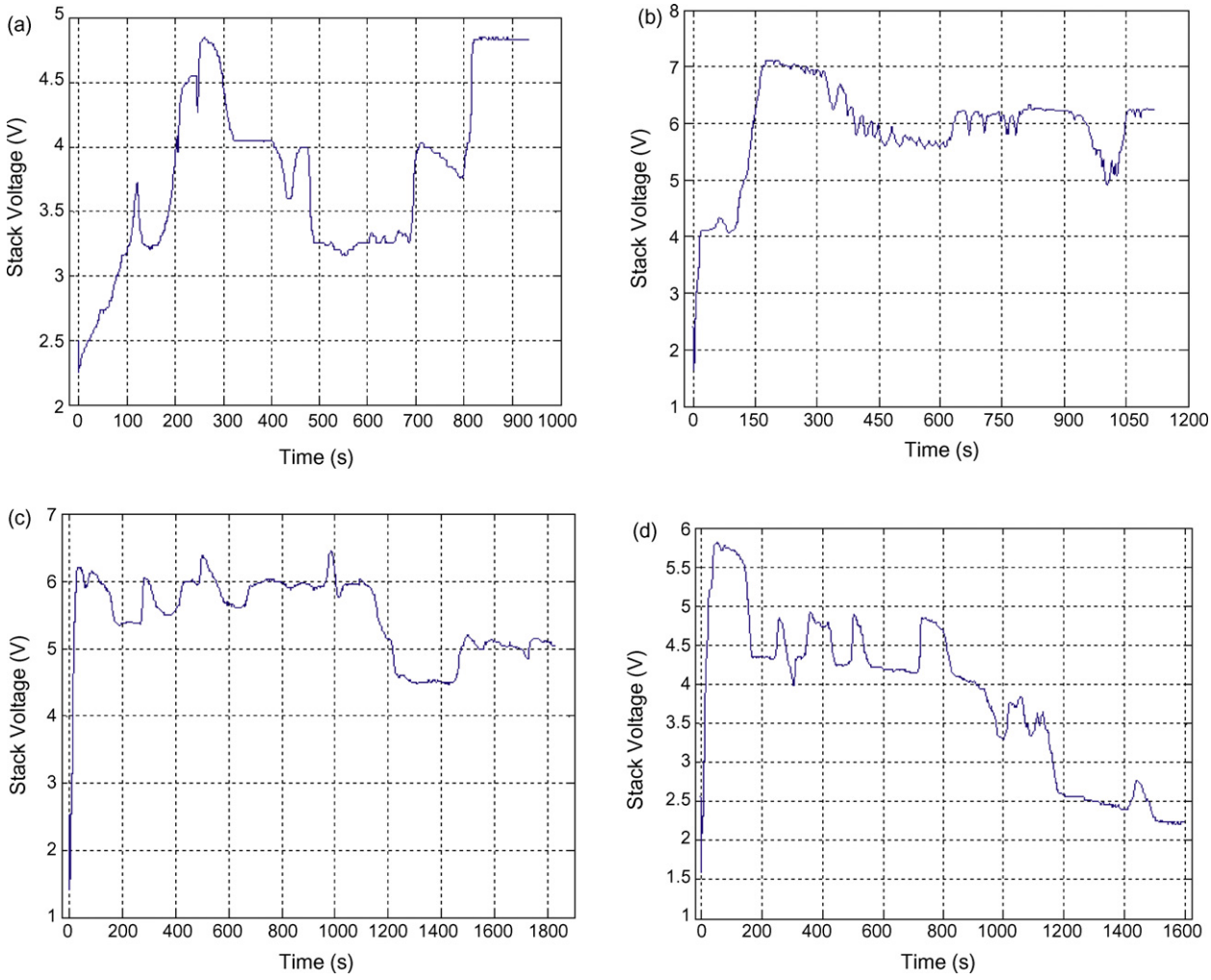

Fig. 10. (a) Stack voltage response after current step-up from 1 A to 2 A with excess coefficient fixed at 2 for air and 1.2 for hydrogen; (b) stack voltage response after current step-up from 1 A to 3 A with excess coefficient fixed at 2 for air and 1.2 for hydrogen; (c) stack voltage response after current step-up from 1 A to 4 A with excess coefficient fixed at 2 for air and 1.2 for hydrogen; (d) stack voltage response after current step-up from 1 A to 6 A with excess coefficient fixed at 2 for air and 1.2 for hydrogen.

excess coefficient of 2 for air, otherwise the voltage oscillation may not be observed.

3.3.2. Dominant frequency of pressure drop versus stack voltage

Using the same data processing technique and procedure, the dominant frequency of the cathode/anode pressure drop signal in the current step-up cases was also analyzed by comparing with the stack voltage change. Similar relationship between dominant frequency of pressure drop and stack voltage was observed. For reasons of brevity, these plots, which may draw exactly similar conclusions as above, are not presented here.

4. Conclusions

In this study, the steady-state performance and dynamic behavior of a commercial 10-cell fuel cell stack was investigated using a self-developed PEM fuel cell test stand. It was found that when air excess coefficient was fixed at 2, the stack voltage experienced obvious and long-time oscillations after either the stack started from idle to a constant current load or stepped up from 1 A to an elevated current. In order to correlate stack voltage with the cathode/anode pressure drop, the fast Fourier transform technique and specifically designed data processing procedure were applied to find the dominant frequency of pressure drop, which successfully revealed the relationship. The dominant frequency of the cathode pressure drop was observed to predict the abrupt stack voltage increase and decrease. The peak of the dominant frequency of cathode pressure drop was found to be an indication the commencement of cathode water flooding. The phase reverse between the dominant frequency and stack voltage was also observed in the start-up to 2 A and 4 A load cases. These relationships exist because changes of dominant frequency and stack voltage are due to the same physics, that is, the water flooding-removal cycle in the cathode. For the dominant frequency of anode pressure drop, it was a direct indication of the water amount at anode, peak of which could be considered an

indication of sudden presence of water at anode. Such water was usually from the cathode due to back diffusion.

It is potentially possible for the pressure drop signal to be utilized as a diagnostic tool for stack voltage. Furthermore, in a PEM fuel cell power system, the stack output could be predicted by pressure drop signal and then controlled by adjusting the flow rate of reactants. However, for this purpose, more experiments are necessary to collect data for different configurations of fuel cell stack under different operating conditions so that a mathematical model describing such relationship can be developed, which could be most challenging. Additionally, an algorithm to determine the optimum window size in performing fast Fourier transform may also be necessary to guarantee that the dominant frequency information is well retained and less noise is present.

Acknowledgments

Financial support from Auto21^{TM} and NSERC is greatly acknowledged. Technical support from Mr. Andrew Jenner at Department of Mechanical, Automotive and Materials Engineering and Mr. Matthew St. Louis at Department of Civil and Environmental Engineering, University of Windsor is also appreciated.

References

[1] J. Larminie, A. Dicks, Fuel Cell System Explained, John Wiley & Sons, 2003, pp. 22–29.
[2] J. Amphlett, R. Mann, B. Peppley, P. Roberge, A. Rodrigues, J. Power Sources 61 (1996) 183–188.
[3] Y. Shan, S.-Y. Choe, J. Power Sources 158 (2006) 274–286.
[4] W.-M. Yan, C.-Y. Soong, F. Chen, H.-S. Chu, J. Power Sources 143 (2005) 48–56.
[5] S. Shimpalee, W. Lee, J. Zee, H. Naseri-Neshat, J. Power Sources 156 (2006) 355–368.
[6] S. Shimpalee, W. Lee, J. Zee, H. Naseri-Neshat, J. Power Sources 156 (2006) 369–374.
[7] S. Kim, S. Shimpalee, J. Zee, J. Power Sources 135 (2004) 110–121.
[8] S. Kim, S. Shimpalee, J. Zee, J. Power Sources 137 (2004) 43–52.
[9] X. Yu, B. Zhou, A. Sobiesiak, J. Power Sources 147 (2005) 184–195.
[10] H. Wu, P. Berg, X. Li, J. Power Sources 165 (2007) 232–243.
[11] Y. Wang, C.-Y. Wang, Electrochim. Acta 50 (2005) 1307–1315.
[12] Y. Wang, C.-Y. Wang, Electrochim. Acta 51 (2006) 3924–3933.
[13] J. Hamelin, K. Agbossou, A. Laperriere, F. Laurenfuel celle, T. Bose, Int. J. Hydrogen Energy 26 (2001) 625–629.
[14] Q. Yan, H. Toghiani, H. Causey, J. Power Sources 161 (2006) 492–502.
[15] F. Philipps, G. Simons, K. Schiefer, J. Power Sources 154 (2006) 412–419.
[16] F. Barbir, H. Gorgun, X. Wang, J. Power Sources 141 (2005) 96–101.
[17] W. He, G. Lin, T.V. Nguyen, AIChE J. 49 (12) (2003) 3221–3228.
[18] K. Jiao, B. Zhou, P. Quan, J. Power Sources 154 (2006) 124–137.
[19] K. Jiao, B. Zhou, P. Quan, J. Power Sources 157 (2006) 226–243.
[20] Y. Zong, B. Zhou, A. Sobiesiak, J. Power Sources 161 (2006) 143–159.